JOURNAL OF VIROLOGY, Oct. 1997, p. 7353–7360 Vol. 71, No. 10
0022-538X/97/$04.00+0

Three-Dimensional Structural Analysis of Recombinant Rotavirus-Like Particles with Intact and Amino-Terminal-Deleted VP2: Implications for the Architecture of the VP2 Capsid Layer

JEFFREY A. LAWTON,[1] CARL Q.-Y. ZENG,[2] SHARMILA K. MUKHERJEE,[3] JEAN COHEN,[4] MARY K. ESTES,[2] AND B. V. VENKATARAM PRASAD[3]*

Program in Cell and Molecular Biology,[1] Division of Molecular Virology,[2] and Verna and Maars McLean Department of Biochemistry and the W. M. Keck Center for Computational Biology,[3] Baylor College of Medicine, Houston, Texas 77030, and Laboratoire de Virologie et Immunologie Moléculaires, Institut National de la Recherche Agronomique, Domaine de Vilvert, 78352 Jouy-en-Josas Cedex, France[4]

Received 20 March 1997/Accepted 13 June 1997

Rotaviruses are the leading cause of severe infantile gastroenteritis worldwide. These viruses are large, complex icosahedral particles consisting of three concentric capsid layers enclosing a genome of eleven segments of double-stranded RNA (dsRNA). The amino terminus of the innermost capsid protein VP2 possesses a nonspecific single-stranded RNA and dsRNA binding activity, and the amino terminus is also essential for the incorporation of the polymerase enzyme VP1 and guanylyltransferase VP3 into the core of the virion. Biochemical and structural studies have suggested that VP2, and especially the amino terminus, appears to act as a scaffold for proper assembly of the components of the viral core. To locate the amino terminus of VP2 within the core, we have used electron cryomicroscopy and image reconstruction to determine the three-dimensional structures of recombinant virus-like particles that contain either full-length or amino-terminal-deleted forms of VP2 coexpressed with the intermediate capsid protein VP6. A comparison of these structures indicates two significant changes along the inner surface of VP2 in the structure lacking the amino terminus: a loss of mass adjacent to the fivefold axes and a redistribution of mass along the fivefold axes. Examination of the VP2 layer suggests that the proteins are arranged as dimers of 120 quasi-equivalent molecules, with each dimer extending between neighboring fivefold axes. Our results indicate that the amino termini of both quasi-equivalent VP2 molecules are located near the icosahedral vertices.

Rotaviruses are recognized to be the leading cause of severe infantile gastroenteritis worldwide, accounting for an estimated 1 million deaths annually (10). Rotaviruses are large, icosahedral particles having a complex structure consisting of three concentric capsid layers surrounding a genome of 11 segments of double-stranded RNA (dsRNA) (21). The genome segments code for six structural and five nonstructural proteins. The outermost layer in the infectious virus is composed of a major capsid protein VP7 and the hemagglutinin spike protein VP4 (20, 28). The intermediate capsid layer is composed of trimers of VP6 organized on a T=13 (*levo*) icosahedral lattice (23). The innermost capsid layer, composed of a 102-kDa protein VP2, encloses the genomic dsRNA (12). Complexes of the two enzymes VP1 and VP3, which are involved in the transcription of the genome within the intact particle, are anchored to the inner surface of VP2 at the icosahedral vertices (22). Together, the VP2 capsid layer along with the genomic dsRNA and transcription enzyme complexes form the core of the virion.

Biochemical studies using truncated forms of recombinant VP2 in Northwestern blotting experiments have shown that VP2 possesses a nonspecific single-stranded RNA and dsRNA binding activity which resides within a distinct amino-terminal domain encompassed by amino acids 1 to 132 (11). Furthermore, these studies have shown that removal of as few as the first 25 amino acids from the amino terminus of VP2 completely abolishes RNA binding activity, suggesting that the integrity of the complete amino-terminal domain is critical for the conformation of the RNA binding site on VP2. The predicted amino acid sequence of this domain contains several motifs which could potentially form the site of interaction between VP2 and RNA (11, 18). In support of these observations, the structure of the native double-layered particle (DLP) determined by electron cryomicroscopy shows significant interactions between the inner surface of VP2 and the genomic dsRNA near the icosahedral fivefold axes and minor interactions along the icosahedral twofold axes (22). These interactions result in nearly 25% of the genomic dsRNA adopting a highly ordered conformation. Clearly the VP2 capsid layer is highly instrumental in organizing the genomic dsRNA within the core.

Biochemical studies using baculovirus-expressed recombinant virus-like particles (VLPs) containing amino-terminal deleted forms of VP2 coexpressed with VP6 and with various combinations of the core transcription enzymes VP1 and VP3 indicate that VP2 also acts as a scaffold for the proper assembly of these enzymes into the core (29). These studies have shown that removal of the first 25 amino acids from the amino terminus completely prevents the incorporation of VP1 or VP3 into VLPs. Thus, a growing body of evidence suggests that the VP2 capsid protein, and in particular the amino terminus, plays a major role in organizing the major components of the endogenous transcription apparatus—the genomic dsRNA and the VP1-VP3 enzyme complexes—within the core of the virion.

Because of the importance of the amino terminus of VP2 in the organization of the viral core, localization of this region of

* Corresponding author. Mailing address: Department of Biochemistry, Baylor College of Medicine, One Baylor Plaza, Houston, TX 77030. Phone: (713) 798-5686. Fax: (713) 796-9438. E-mail: vprasad@bcm.tmc.edu.

the protein within the intact particle may provide insights not only into the architecture of the VP2 capsid layer but also into two key processes which occur during the viral life cycle: endogenous genome transcription inside the DLP and assembly of the progeny core during virus maturation. We have used electron cryomicroscopy and computer image processing to determine the three-dimensional structure of a baculovirus-expressed recombinant VLP containing VP6 and a genetically truncated form of VP2 in which amino acids 1 to 92 have been removed (Δ2/6-VLP). Using difference map analysis to compare this structure with those of the native 2/6-VLP (previously called VLP-2/6 [22]) and the transcriptionally competent DLP, we have defined the probable locations of the VP2 amino termini within the core and identified conformational changes which occur at the inner surface of the VP2 layer when the transcription complexes and genomic dsRNA are present. This work has also provided insight into the general organization of the VP2 capsid layer, allowing us to propose that quasi-equivalent molecules of VP2 are arranged as 60 dimers on a T=1 icosahedral lattice.

MATERIALS AND METHODS

Preparation of DLP, 2/6-VLP, and Δ2/6-VLP specimens. Native rotavirus DLPs of strain SA11-4F were prepared by EDTA treatment of infectious virions harvested from MA-104 cells as described earlier (23). VLPs containing full-length VP2 and VP6 (2/6-VLP) were produced in *Spodoptera frugiperda* 9 (Sf9) cells by using the baculovirus expression system as described earlier (3). VLPs containing the amino-terminal truncated form of VP2 were prepared as described elsewhere (29). Briefly, the full-length VP2 cDNA was cleaved at the Gln_{92}-Lys_{93} codon junction, and the resulting C-terminal fragment was ligated into an appropriate baculovirus expression vector. This recombinant baculovirus construct was coexpressed along with full-length VP6 in Sf9 cells. Δ2/6-VLPs were purified by density gradient centrifugation and suspended in TNC buffer (10 mM Tris [pH 7.4], 140 mM NaCl, 10 mM $CaCl_2$) at a concentration of $\sim 10^{12}$ particles/ml.

Sodium dodecyl sulfate-polyacrylamide gel electrophoresis characterization of VLP specimens. The protein composition of 2/6-VLPs and Δ2/6-VLPs was confirmed by sodium dodecyl sulfate-polyacrylamide gel electrophoresis analysis using a 12% resolving and 4% stacking polyacrylamide gel as described previously (13). Protein bands were visualized by using a silver-staining kit (Sigma) according to the manufacturer's instructions.

Electron cryomicroscopy. Specimens for microscopy were embedded in a thin layer of vitreous ice on holey carbon films, using standard procedures (6). Frozen hydrated specimens were imaged in a JEOL 1200 electron cryomicroscope, using a 100-kV electron beam with a dose of ~ 5 $e^-/Å^2$ at a magnification of ×30,000. Images were collected on Kodak SO-163 electron film with a 1-s exposure time. Micrographs were developed for 12 min in Kodak D-19 developer at 21°C and fixed for 10 min in Kodak fixer. For structure determination, separate images of 2/6-VLPs and Δ2/6-VLPs were collected at ~0.9-μm underfocus; for size comparison, Δ2/6-VLPs and DLPs were imaged together at ~1.3-μm underfocus. The defocus value of each micrograph was estimated from the positions of the contrast transfer function rings in the sum of individual particle image Fourier transforms (32).

Three-dimensional structural analysis. Micrographs were chosen for structural analysis based on the criteria of ice quality, particle concentration, and optimum defocus. Images were digitized with a Perkin-Elmer microdensitometer at a raster scanning interval of 5.33 Å in the object. The three-dimensional reconstructions were generated by using the software in the ICOS Toolkit suite (14). Briefly, individual particle images were selected from the digitized micrographs by using the program boxmrc (9). For the VLP reconstructions, particle centers were estimated by cross-correlation with a rotationally averaged reference projection (19) prepared from a previously derived reconstruction of the 2/6-VLP (22). For each particle, a set of 13 potential orientations with phase-minimized centers were estimated based on self-common lines (4, 7, 14). The most likely orientation for each particle was selected by cross-common lines comparison (7) of these 13 orientations with a set of seven reference projections prepared from the previous reconstruction of 2/6-VLP. Once an initial set of particle orientations was assembled, a preliminary reconstruction was generated by the cylindrical expansion method of Crowther (4). The set of particle orientations was then refined by cross-common lines based conjugate gradient refinement (7) of each orientation against a set of seven reference projections of the preliminary reconstruction. Centers were refined by reciprocal space cross-correlation of each particle image with its projection. Using the refined orientations and centers, a new reconstruction was generated, and the refinement process was repeated iteratively. The DLP reconstruction was produced in the same way except that a previously derived reconstruction of DLP was used for the starting reference projections (22).

The resolution achieved in each of the final structure determinations was assessed by Fourier ring correlation analysis (27). For this assessment, the set of particle images used in the final reconstruction was divided into two groups from which independent reconstructions were generated. These two reconstructions were compared in Fourier space by computing the mean phase residual and cross-correlation coefficient as a function of resolution. The resolution limit of the structure was taken to be the point in Fourier space where the mean phase residual between the two reconstructions exceeded 45°. At this point, the Fourier cross-correlation coefficient was typically between 0.60 and 0.65.

Reconstructions were viewed on a Silicon Graphics workstation, using IRIS Explorer 3.5 (Numerical Algorithms Group, Inc.) in conjunction with several customized visualization modules (15). For each structure, the appropriate surface electron density contour level was chosen to account for approximately 780 molecules of VP6 between the radii 260 Å and 350 Å (22). For some analyses, electron density contour levels were expressed in terms of standard deviation (σ) from the mean of the reconstruction. Corrections for the effects of the contrast transfer function were not performed on any of the final reconstructions, as the portions of the image Fourier transforms used were within the first zero of the contrast transfer function in each case.

Difference map analysis. To identify regions of dissimilarity between the 2/6-VLP and Δ2/6-VLP structures, difference maps were prepared by using software in the ICOS Toolkit suite. Briefly, the two structures were radially scaled by alignment of radial density profiles to correct for any slight magnification differences, and electron density levels were normalized to achieve equal mass density in the VP6 regions. Difference maps were computed by arithmetic subtraction of the electron density values within the protein regions voxel for voxel in the two structures. By alternating the order of subtraction of the two structures, the differences between the 2/6-VLP and Δ2/6-VLP structures was deconvoluted into two independent maps such that each showed only those structural features which could be attributed to one of the two structures.

RESULTS

Characterization of Δ2/6-VLPs by electron cryomicroscopy. Purified Δ2/6-VLPs were mixed with native DLPs as an internal standard and imaged by electron cryomicroscopy (Fig. 1). These two particle types may be easily distinguished in the micrograph, as the DLPs appear substantially darker due to the presence of RNA inside the core. The Δ2/6-VLPs appeared to have a uniform morphology and an overall diameter similar to that of the native DLPs. To determine whether the overall diameter of the Δ2/6-VLP is identical to that of the DLP, as has been previously observed for the native 2/6-VLP (22), three-dimensional reconstructions of both particle types were computed to a nominal resolution of 22 Å, using 78 DLP images and 30 VLP images. In both cases, 100% of the mean inverse eigenvalue spectrum (as described by Crowther et al. [5]) was below 0.1. Because both particle types were imaged together in the same micrograph, the imaging conditions and especially the magnification applied to both specimens were identical. Averaged radial density profiles confirmed that the VP2 and VP6 capsid layers are positioned at the same radii in both structures (data not shown). These results indicate that for all three types of particles examined, 2/6-VLP, Δ2/6-VLP, and DLP, the overall dimensions of the capsid layers are identical.

Three-dimensional structures of the 2/6-VLP and Δ2/6-VLP. To identify differences between the 2/6-VLP and Δ2/6-VLP structures which may suggest the locations of the amino termini of VP2 within the viral core, purified VLPs of both types were imaged separately by electron cryomicroscopy. Imaging of these two types of VLPs together was not done because of the difficulty in distinguishing 2/6-VLPs from Δ2/6-VLPs in a micrograph. To determine the structure of the Δ2/6-VLP, a three-dimensional reconstruction was computed to a resolution of 22 Å, using 230 particle images. The distribution of particle orientations covering the asymmetric unit was sufficient for the resolution attained in the reconstruction, as 98% of the mean inverse eigenvalue spectrum was less than 0.01. The resolution was confirmed by Fourier ring correlation analysis (27).

For comparison purposes, a reconstruction of the 2/6-VLP

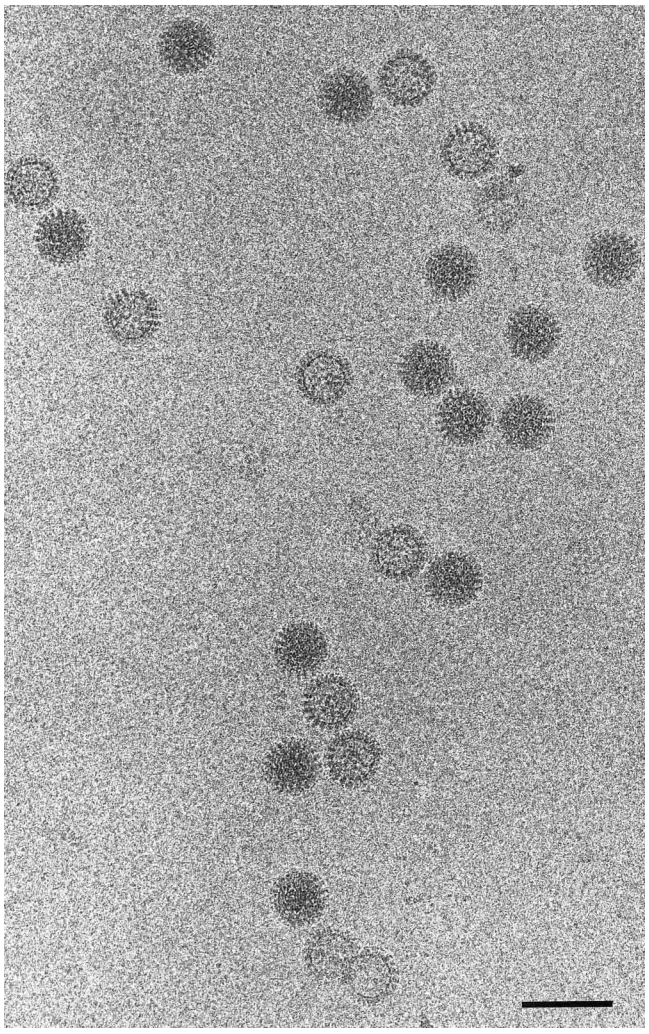

FIG. 1. Electron cryomicrograph of DLPs and Δ2/6-VLPs (scale bar, 1,000 Å). Native DLPs appear darker because of the presence of genomic dsRNA within the core. The Δ2/6-VLPs appear to have a uniform morphology which is very similar to that observed for 2/6-VLPs (22). The overall diameters of the two particle types appear to be identical.

was also computed to a resolution of 22 Å by using 182 particle images, with 99% of the mean inverse eigenvalue spectrum falling below 0.01. The surface representations of these two VLP structures are shown in Fig. 2.

Comparison of VLP-2/6 and VLP-Δ2/6 structures. The overall architectures of the VP6 capsid region were identical in the two structures (Fig. 2a), as was expected because both VLPs contain native VP6. Deconvoluted difference maps (see Materials and Methods) between these two structures were computed to identify regions of dissimilarity within the VP2 capsid layer between the two VLPs (Fig. 2c). These difference maps, which were computed to show differences in mass density greater than 0.75 σ, indicated that all of the significant architectural differences between 2/6-VLP and Δ2/6-VLP were concentrated near the icosahedral vertices at the inner surface of VP2. These features have been consistently seen in three independent structural determinations using two separate VLP preparations. The locations of these structural differences suggest that the effect of removing the amino terminus of VP2 is to disrupt the normal architecture of the VP2 layer in the vicinity of the icosahedral vertices.

Along the inner surface of VP2 in the 2/6-VLP structure, the region surrounding the icosahedral vertex appeared to protrude slightly inward, creating a pentagonal star-like structure with spokes radiating outward from the fivefold axis (Fig. 2b, left panel). The smaller inwardly protruding mass density at the fivefold axis itself was essentially flat. These observations are entirely consistent with the architecture of the icosahedral vertices reported earlier for 2/6-VLP (22).

In the corresponding region of the Δ2/6-VLP structure in which the amino-terminal 92 amino acids of VP2 were deleted, the star-like configuration surrounding the icosahedral vertex appeared to undergo a conformational change resulting in a structure which more closely resembled an array of fan blades radiating outward from the fivefold axis (Fig. 2b, right panel). Where the region along the fivefold axis itself was relatively flat in the 2/6-VLP structure, a small portion of the VP2 mass density appeared to extend further inward by an additional 20 Å along the fivefold axis in the Δ2/6-VLP structure. The unexpected appearance of additional mass relative to 2/6-VLP at this location in the Δ2/6-VLP structure may be the result of a conformational change in the VP2 capsid following the removal of the amino terminus, causing some of the remaining residues of VP2 to relocate to the fivefold axis from elsewhere in the vicinity of the icosahedral vertex.

The structural differences between 2/6-VLP and Δ2/6-VLP were all observed to occur along the interior surface of the VP2 capsid layer in the vicinity of the icosahedral vertices (Fig. 2c). Taken together with the observation that the amino terminus of VP2 makes contact with the genomic dsRNA and is required for the incorporation of the VP1-VP3 enzyme complexes into the core of the virion, these results imply that the amino termini of VP2 are located near the fivefold axes and are likely positioned along the inner surface to interact with the core components of the virion.

Arrangement of VP2 molecules within the capsid layer. To define the relationship between the locations of mass differences observed between the two VLPs and the distribution of individual VP2 molecules within the capsid layer, the VP2 region within the Δ2/6-VLP structure was examined to define the arrangement and stoichiometry of VP2 monomers. At the surface electron density contour level which accounts for 780 molecules of VP6 between the radii 260 Å and 350 Å (0.4 σ), the VP2 capsid layer in the Δ2/6-VLP structure appeared as a relatively smooth contiguous shell (Fig. 3a). Volume calculations suggested that there are approximately 120 molecules of VP2 present within the region of the capsid between 230 and 260 Å in the native 2/6-VLP and in the DLP, as suggested earlier (25). This stoichiometry is consistent with biochemical estimates based on metabolic labeling studies of rotavirus proteins (17). The stoichiometry of 120 VP2 molecules in the capsid layer suggests that the proteins are likely arranged as 60 dimers on a T=1 icosahedral lattice. However, at a threshold of 0.4 σ, the boundaries between individual VP2 monomers could not be distinguished.

To delineate the approximate boundaries between VP2 molecules, the VP2 region within the Δ2/6-VLP structure was examined at various elevated electron density contour thresholds. Although this analysis does not always permit a clear distinction to be made between adjoining protein monomers, the capsid region nonetheless may be clearly divided into morphologically distinct subunits. The Δ2/6-VLP structure was chosen over that of the native 2/6-VLP for this analysis because the removal of the amino terminus of VP2 allows the boundaries between the capsid subunits in the VP2 layer to be visu-

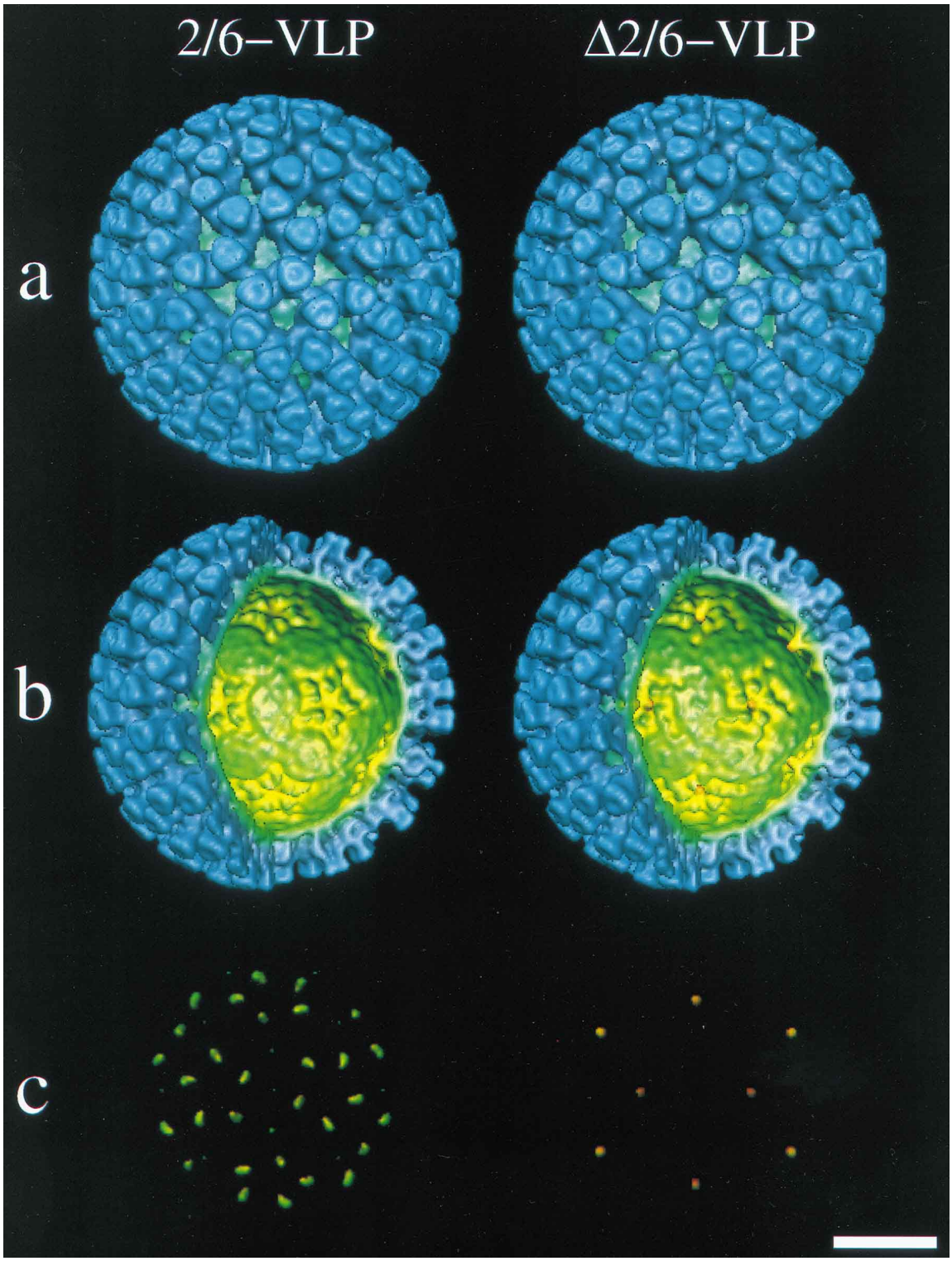

FIG. 2. Three-dimensional structures of 2/6-VLP and Δ2/6-VLP at 22-Å resolution, viewed along the icosahedral twofold axis and radially depth-cued in color according to the color chart shown in Fig. 4. (a) Surface topology of the particle exteriors, contoured to yield ~780 molecules of VP6 between the radii 260 Å and 350 Å. (b) Partial cross sections of the particles, showing the topology of the inner surface of the VP2 capsid layer. The icosahedral vertices are at the locations where VP2 protrudes inward, forming a star-like pentagonal configuration in the 2/6-VLP and a fan blade configuration in the Δ2/6-VLP. This cross-section provides views of the icosahedral vertex from three different perspectives. (c) Deconvoluted difference maps between the 2/6-VLP and Δ2/6-VLP structures, indicating which features are present in one structure and absent in the other. For clarity, only the back hemispheres of the difference maps are shown. The VP2 regions reveal two types of differences in the topology of the VP2 inner surface at the icosahedral vertices. The VP6 regions of the difference maps are essentially clean. Scale bar, 200 Å.

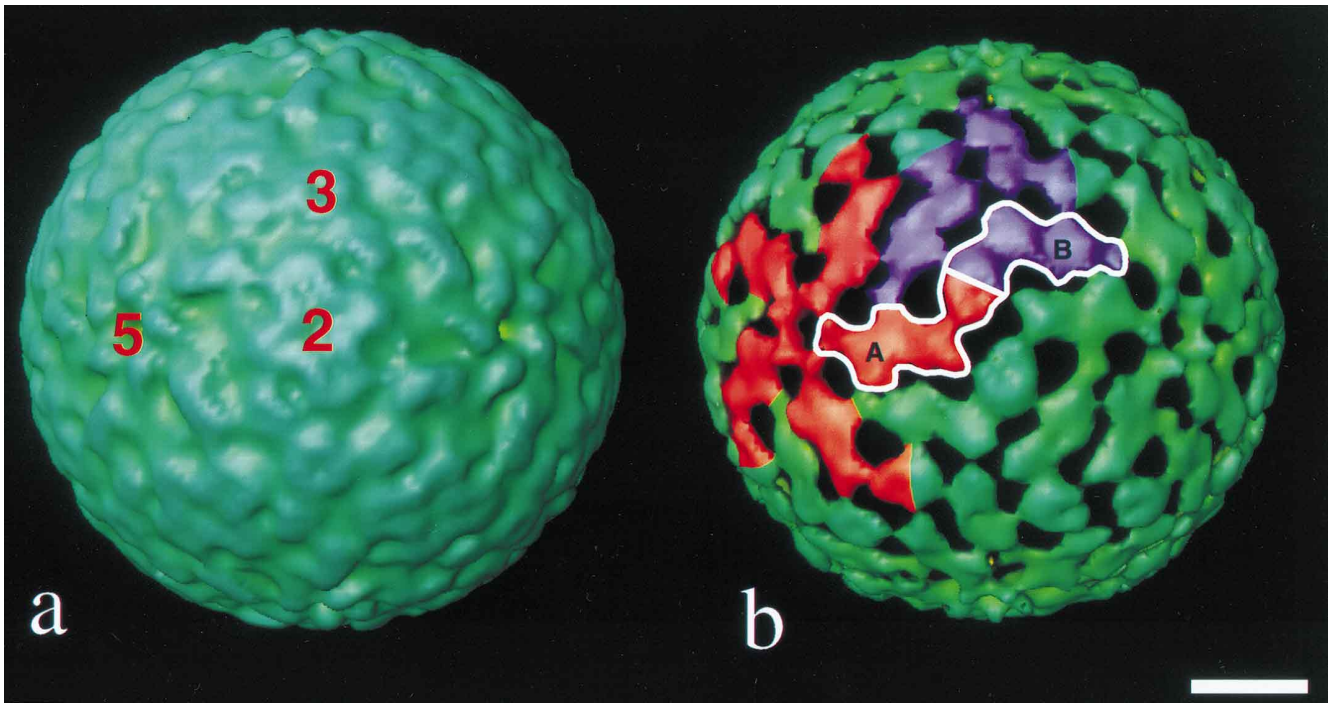

FIG. 3. Proposed arrangement of quasi-equivalent VP2 monomers. (a) Surface topology of the VP2 capsid layer in the Δ2/6-VLP structure, computationally isolated from the reconstruction and viewed at a surface electron density contour level of ~0.4 σ, which corresponds to a threshold yielding ~780 molecules of VP6 in the outer capsid region. The surface of the VP2 layer is relatively smooth and unbroken, as has been previously observed for 2/6-VLP (22). Volume calculations predict that this surface encloses ~120 molecules of VP2, assuming a uniform protein density of 1.30 g/cm^3. The locations of three of the principle icosahedral axes are indicated in red. (b) Surface topology of the VP2 capsid layer at a higher contour level (~2.3 σ), showing how the capsid layer breaks up into 60 equivalent strips of mass extending between adjacent fivefold axes. These strips appear to have a pseudo-twofold axis of symmetry in the center, consistent with the proposal that each strip is composed of a dimer of quasi-equivalent VP2 molecules. Based on the comparison of these strips of mass with the locations of quasi-equivalent inner capsid proteins proposed for aquareovirus (26) and shown at atomic resolution for bluetongue virus (8), both of which are structurally similar to rotavirus, the two types of quasi-equivalent VP2 molecules may be arranged such type A monomers (red) extend between fivefold and twofold axes and type B monomers (purple) extend between fivefold and threefold axes. Scale bar, 100 Å.

alized more definitively. At a contour threshold of 2.3 σ, the surface of VP2 appeared to break up into 60 narrow strips of mass density which stretched between neighboring fivefold axes, consistent with the proposal that the asymmetric unit of the VP2 capsid layer is organized on a T=1 icosahedral lattice, with each dimer extending from a fivefold axis proper across the surface to a point near an adjacent fivefold axis (Fig. 3b).

This strip of mass density, which at a contour level of 2.3 σ comprises the morphological asymmetric unit of the VP2 surface, appeared to have an approximate center of symmetry which corresponds to a pseudo-twofold axis. This center of symmetry divides the asymmetric unit of the VP2 capsid layer into two halves of roughly equal volume. We propose that these two halves may correspond to the two quasi-equivalent monomers of VP2 which together compose the asymmetric unit of the capsid layer. These two quasi-equivalent monomers have been designated types A and B, with type A extending from the icosahedral fivefold axis proper to the icosahedral twofold and type B extending from a point adjacent to the fivefold axis to the icosahedral threefold.

Interestingly, the two types of significant mass differences observed in the difference maps—the extension of VP2 mass density further inward along the fivefold axes in the Δ2/6-VLP structure and the small pieces of mass density adjacent to the fivefold axes which are missing in the Δ2/6-VLP structure—appeared to be very close to the ends of the type A and type B monomers, respectively. This observation suggests that amino termini of both types of quasi-equivalent VP2 monomers are in the vicinity of the icosahedral vertices, with one amino terminus very close to the fivefold axis and the other slightly offset.

Comparison of the Δ2/6-VLP and DLP structures. To understand how the removal of the amino terminus of VP2 affects RNA binding activity, and in particular to visualize how the structural alterations observed around the icosahedral vertices in the VP2 region of the Δ2/6-VLP structure relate to the interactions observed between RNA and the inner surface of VP2 in the DLP, the VP2 regions surrounding the icosahedral vertices were computationally isolated from the DLP and the two VLP structures (Fig. 4). Consistent with earlier structural studies, the star-shaped pentagonal configuration seen on the inner surface of VP2 in the 2/6-VLP structure appeared to be similar overall in the DLP (22).

Around each vertex in the DLP, three classes of symmetrically related interactions between RNA and VP2 appeared as inward protrusions of mass density extending 5 to 10 Å into the core (indicated as 1, 2, and 3 in Fig. 4c). A comparison of the DLP vertex region with the predicted arrangement of VP2 monomers around the vertex (Fig. 4d) indicated that the class 1 connections may be mediated by the type A monomers of VP2, while those of class 2 are likely mediated by type B monomers. Interestingly, these two classes of protein-RNA interactions were of equal distance from the fivefold axis and lay immediately adjacent to the portion of VP2 mass density which was observed to be missing in the Δ2/6-VLP structure (Fig. 2c, left panel). The class 3 interactions, which were observed to occur nearer to the fivefold axis than the other two

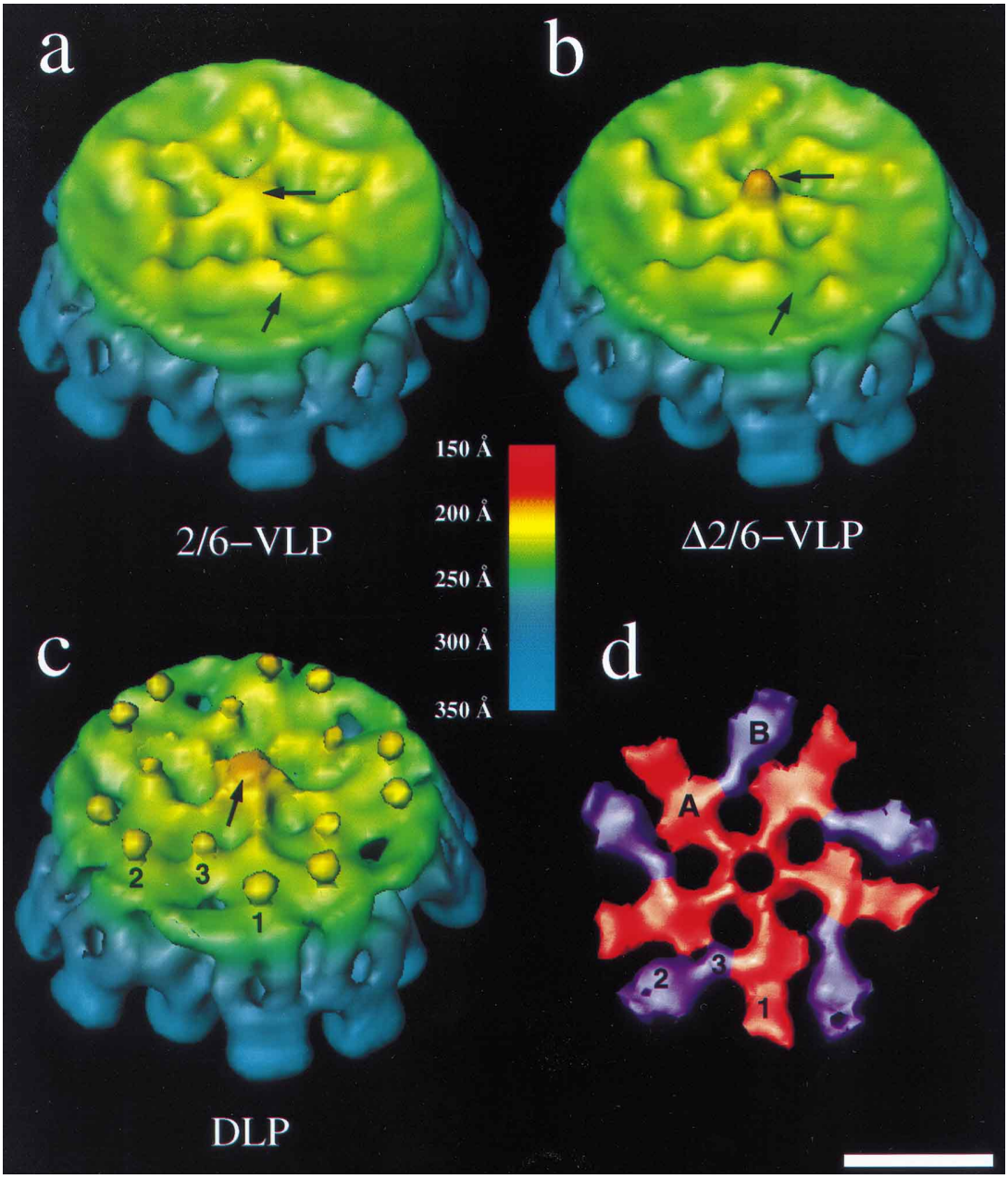

FIG. 4. Comparison of icosahedral vertices in 2/6-VLP, Δ2/6-VLP, and DLP structures showing the interactions between VP2 and dsRNA. One of the icosahedral vertices has been computationally isolated from each structure and inverted to reveal the topology of the inner surface of VP2. The isolated vertices shown in panels a to c have been radially colored according to the color chart and tilted slightly to illustrate the topology, while in panel d, the VP2 region of the vertex from Δ2/6-VLP has been displayed at high contour and colored as in Fig. 3 to illustrate the proposed arrangement of the portions of the type A and type B monomers which lie in the vicinity of the icosahedral vertex. Scale bar, 100 Å. (a) Vertex isolated from the 2/6-VLP structure, showing the pentagonal star-shaped configuration of ridges surrounding the fivefold axis. Arrows indicate where mass density differences exist between 2/6-VLP and Δ2/6-VLP in this region, as identified by the difference maps shown in Fig. 2c. (b) Vertex isolated from the Δ2/6-VLP structure in which the star-shaped configuration of ridges has undergone a conformational change to resemble an array of fan blades radiating outward from the fivefold axis. As in panel a, arrows indicate the locations of mass density differences following this conformational change. The extra mass at the fivefold axis is likely the result of a rearrangement in which some of the remaining residues in the truncated form of VP2 relocate to the fivefold axis from elsewhere in the vicinity of the icosahedral vertex. (c) In the vertex isolated from the DLP, much of the VP1-VP3 transcription enzyme complex (which extends from the orange protrusion at the fivefold axis in the center, indicated by arrow) and the surrounding regions of genomic dsRNA have been removed for clarity. Three distinct classes of protein-RNA interactions (marked as 1, 2, and 3) are visible surrounding the fivefold axis in the DLP structure. (d) The corresponding VP2 region surrounding the fivefold axis in Δ2/6-VLP, displayed at high contour and colored as in Fig. 3 to illustrate the proposed locations of VP2 monomers at the vertex. Type A monomers are shown in red, and type B monomers are shown in purple. The locations of protein-RNA connections seen in the DLP near the vertex are marked as 1, 2, and 3.

classes, may be formed by either A or B monomers. These bservations suggested that the amino terminus of each of the 120 VP2 molecules may mediate at least one interaction with RNA. None of these observed protein-RNA interactions coincided precisely with the locations of the conformational changes seen in the Δ2/6-VLP structure, suggesting that the removal of the first 92 amino acids from VP2, while disrupting the normal interactions with RNA, did not

completely remove the protein domains responsible for the interactions.

The inner surface of VP2 near each of the interactions with RNA in the DLP appeared to be altered in several ways such that either a small channel opened up through the capsid layer or the layer itself appeared to be much thinner than those in 2/6-VLP or Δ2/6-VLP structures. These small differences may be the result of conformational changes which occur in the VP2 layer when RNA is bound. It is not known whether the observed connections are composed of VP2 extending inward to contact the RNA or vice versa.

DISCUSSION

The results of biochemical studies on the architecture of the viral core in rotavirus suggest that the inner capsid protein VP2 serves as a scaffold for the proper assembly of the genomic dsRNA and the transcription enzymes VP1 and VP3 into the core (11, 29). The role of VP2 as a scaffold may be especially important during the process of genome transcription, which occurs within structurally intact DLPs early in the replication cycle (21). The structural integrity of the DLP is required for efficient genome transcription (2), suggesting that VP2, through its interactions with the components of the transcription machinery in the core, may be essential for maintaining the proper arrangements of the RNA and the enzymes during repeated initiation-elongation cycles (16). As VP2 is the only rotavirus structural protein believed to be capable of self-assembling into a stable capsid (3, 12), these interactions may also be critical for the proper inclusion of the genome and the transcription enzymes into progeny particles during virus morphogenesis (11, 31).

These critical interactions appear to be mediated by amino acids located within the amino terminus of VP2. The location of the amino terminus of VP2 within the intact core is not known. However, expression of native VP6 along with a genetically truncated form of VP2 lacking the first 92 amino acids in the baculovirus system gives rise to recombinant VLPs. VLPs containing such a form of VP2 lack the ability to incorporate the transcription enzymes VP1 and VP3 (29) and also likely cannot interact with RNA, as the RNA binding region of VP2 is nearly all missing. Interestingly, naturally occurring empty DLPs isolated from infected cells contain a cleaved form of VP2 (1) which Zeng et al. (30) suggested probably lacks the amino terminus. Our three-dimensional structural analysis of Δ2/6-VLPs which contain a truncation of the first 92 amino acids of VP2 suggests that the amino termini are clustered around the 12 icosahedral vertices, with the RNA binding domains facing inward.

The anticipated effect of removing the amino terminus of VP2 would be an apparent loss of mass in the Δ2/6-VLP structure. In the difference map identifying the features present in 2/6-VLP but absent in Δ2/6-VLP (Fig. 2c, left panel), the small pieces of mass density surrounding each icosahedral vertex correspond to those portions of the star-like configuration of 2/6-VLP which, being absent in the Δ2/6-VLP structure, give rise to the fan blade configuration. These pieces of mass density may represent structurally discernible portions of VP2 amino termini which are missing in the Δ2/6-VLP structure; alternatively, they may represent conformational changes within the VP2 layer which occur because of the removal of the amino terminus. Volume calculations indicate that these pieces of mass density do not account for the entire expected mass difference resulting from the removal of the first 92 amino acids from VP2, suggesting that the amino terminus may be partially disordered, and hence only partially visible, in the native structure.

The other major architectural difference observed between the two VLPs involves the additional extension of VP2 mass density further inward along the fivefold axes in the structure lacking the amino terminus of VP2 (Fig. 2c, right panel). This unexpected observation is likely the result of a conformational rearrangement which occurs in the architecture of the VP2 capsid in the absence of the amino terminus, perhaps causing a small portion of the remaining VP2 to relocate to the fivefold axis from its normal position elsewhere in the capsid. Interestingly, this rearrangement occurs at the location of the interaction between VP2 and the transcription enzyme complex observed in the native DLP (22). These changes in the virus architecture probably explain why removal of the amino terminus of VP2 prevents incorporation of the transcription enzymes into the core.

To understand how the observed architectural differences between 2/6-VLP and Δ2/6-VLP relate to the distribution of individual VP2 monomers within the capsid, we have examined the VP2 capsid region at a surface electron density contour level which allows the boundaries between morphological units to become apparent. The asymmetric unit of the VP2 capsid layer appears as a strip of mass density which originates at one fivefold axis and extends to a point near a neighboring fivefold axis. These 60 units are organized on a T=1 icosahedral lattice. Because both volume calculations and biochemical studies suggest there to be 120 molecules of VP2 present in the capsid (17), and there are 60 structurally equivalent morphological units making up the capsid, each unit is likely composed of two VP2 molecules.

The proposed dimeric arrangement of quasi-equivalent VP2 monomers on a T=1 icosahedral lattice is shown in Fig. 3. Type A monomers originate at the fivefold axis and extend to the twofold, while type B monomers originate at a point near the fivefold and extend around the threefold. Structural studies of other segmented dsRNA viruses within the family *Reoviridae* have noted a similar arrangement of monomers within the inner capsid layer. In the three-dimensional structure of aquareovirus determined by electron cryomicroscopy, Shaw et al. (26) observed that the asymmetric unit of the innermost capsid layer is composed of subunits organized as dimers on a T=1 icosahedral lattice, as seen in both surface representations and radial projections of the capsid region. In the structurally related bluetongue virus, X-ray crystallographic studies have shown at atomic resolution that the innermost capsid protein VP3 is organized as dimers on T=1 icosahedral lattice in an arrangement similar to that proposed here for VP2 (8). This correspondence is not surprising, because the two proteins VP3 in bluetongue virus and VP2 in rotavirus have nearly identical molecular weights and form shells having similar dimensions (24).

Where are the amino termini of these two types of quasi-equivalent monomers located within the core? The small additional protrusion of mass along the fivefold axis in the Δ2/6-VLP structure is located at the point where five type A monomers meet at the icosahedral vertex (Fig. 4d). In the same way, the small losses of mass seen in the Δ2/6-VLP structure adjacent to the fivefold axis are located very close to the ends of the five type B monomers surrounding the icosahedral vertex. These observations are consistent with the proposal that the type A amino termini are located at or very near the fivefold axes themselves, interacting in a head-to-head configuration, and the type B amino termini are located slightly offset from the fivefold axes. Because their architectural environments are not the same within the capsid, the amino ter-

mini of the two quasi-equivalent VP2 molecules probably have slightly different conformations.

Localization of the amino termini near the fivefold axes does not imply that the carboxy termini of the type A and B monomers are located at the icosahedral two- and threefold axes, respectively, where the two types of monomers appear to form intermolecular interactions with one another. Further mutagenesis and structural studies are required to locate the carboxy termini of VP2 in rotavirus.

In addition to providing a scaffold for the assembly of the transcription enzymes within the core, VP2 also interacts with the genomic dsRNA, as demonstrated in biochemical and structural studies. In the native DLP, the strongest interactions are observed within the vicinity of the icosahedral vertices. The fact that there are 15 protein-RNA contacts and 10 VP2 monomers present around each vertex suggests that each VP2 monomer in the capsid likely interacts with RNA. Based on the proposed arrangement of VP2 monomers within the capsid, Fig. 4c illustrates the way in which both types of monomers may be responsible for the three classes of protein-RNA contacts observed within the vicinity of the icosahedral vertex.

Interestingly, the overall topology of the inner surface of VP2 in the immediate vicinity of the observed protein-RNA interactions appeared to be quite similar in all three structures. In the Δ2/6-VLP structure, the changes resulting from the removal of the amino termini of VP2 were located near, but not precisely at, the positions of these connections. This observation suggests that the domain of VP2 which mediates the interaction with RNA, while perhaps still present to some degree in the Δ2/6-VLP structure, nevertheless undergoes a conformational change which renders it unable to interact properly with RNA.

While the two types of VP2 monomers appear to form similar interactions with the genomic dsRNA within the core, this is likely not the case with the transcription enzymes. Because the VP1-VP3 complexes are anchored to the inner surface of the VP2 capsid layer along the fivefold axes, the binding site is probably formed exclusively by type A monomers of VP2, as these appear to interact in a head-to-head configuration at the fivefold axes (Fig. 4d). This observation suggests that the scaffolding roles for the two types of quasi-equivalent VP2 molecules are slightly different with respect to the major components of the transcription machinery within the core of the virion.

ACKNOWLEDGMENTS

This research was supported by NIH grants AI-36040 (B.V.V.P.) and DK-30144 (M.K.E.) and by the R. Welch Foundation. J.A.L. acknowledges the support of training grant GM-08280 from the National Institute of General Medical Sciences.

We thank D. Stuart for sharing unpublished results on the structure of bluetongue virus.

REFERENCES

1. **Brüssow, H., A. Bruttin, and S. Marc-Martin.** 1990. Polypeptide composition of rotavirus empty capsids and their possible use as a subunit vaccine. J. Virol. **64:**3635–3642.
2. **Cohen, J.** 1977. Ribonucleic acid polymerase activity associated with purified calf rotavirus. J. Gen. Virol. **36:**395–402.
3. **Crawford, S. E., M. Labbé, J. Cohen, M. H. Burroughs, Y.-J. Zhou, and M. K. Estes.** 1994. Characterization of virus-like particles produced by the expression of rotavirus capsid proteins in insect cells. J. Virol. **68:**5945–5952.
4. **Crowther, R. A.** 1971. Procedures for the three-dimensional reconstruction of spherical viruses by Fourier synthesis from electron micrographs. Philos. Trans. R. Soc. Lond. B **261:**221–230.
5. **Crowther, R. A., D. J. DeRosier, and A. Klug.** 1970. The reconstruction of a three-dimensional structure from projections and its applications to electron microscopy. Proc. R. Soc. Lond. A **317:**319–340.
6. **Dubochet, J., et al., and P. Schultz.** 1988. Cryo-electron microscopy of vitrified specimens. Q. Rev. Biophys. **21:**129–228.
7. **Fuller, S. D.** 1987. The T=4 envelope of Sindbis virus is organized by interactions with a complementary T=3 capsid. Cell **48:**923–934.
8. **Grimes, J., P. Mertens, and D. Stuart.** Personal communication.
9. **Hardt, S., and B. V. V. Prasad.** Unpublished data.
10. **Kapikian, A. Z., and R. M. Chanock.** 1996. Rotaviruses, p. 1657–1708. *In* B. N. Fields, D. M. Knipe, R. M. Chanock, J. L. Melnick, B. Roizman, and R. E. Hope (ed.), Virology. Raven Press, New York, N.Y.
11. **Labbé, M., P. Baudoux, A. Charpilienne, D. Poncet, and J. Cohen.** 1994. Identification of the nucleic acid binding domain of the rotavirus VP2 protein. J. Gen. Virol. **75:**3423–3430.
12. **Labbé, M., A. Charpilienne, S. E. Crawford, M. K. Estes, and J. Cohen.** 1991. Expression of rotavirus VP2 produces empty corelike particles. J. Virol. **65:**2946–2952.
13. **Laemmli, U. K.** 1970. Cleavage of structural proteins during the assembly of the head of bacteriophage T4. Nature **277:**680–685.
14. **Lawton, J. A., and B. V. V. Prasad.** 1996. Automated software package for icosahedral virus reconstruction. J. Struct. Biol. **116:**209–215.
15. **Lawton, J. A., and B. V. V. Prasad.** Unpublished data.
16. **Lawton, J. A., M. K. Estes, and B. V. V. Prasad.** 1997. Three-dimensional visualization of mRNA release from actively-transcribing rotavirus particles. Nat. Struct. Biol. **4:**118–121.
17. **Liu, M., P. A. Offit, and M. K. Estes.** 1988. Identification of the simian rotavirus SA11 genome segment 3 product. Virology **163:**26–32.
18. **Mitchell, D. B., and G. W. Both.** 1990. Completion of the genomic sequence of the simian rotavirus SA11: nucleotide sequences of segments 1, 2 and 3. Virology **177:**324–331.
19. **Olson, N. H., and T. S. Baker.** 1989. Magnification calibration and the determination of spherical virus diameters using cryoEM. Ultramicroscopy **30:**281–298.
20. **Prasad, B. V. V., J. W. Burns, E. Marietta, M. K. Estes, and W. Chiu.** 1990. Localization of VP4 neutralization sites in rotavirus by three-dimensional cryo-electron microscopy. Nature **343:**476–479.
21. **Prasad, B. V. V., and M. K. Estes.** 1997. Molecular basis of rotavirus replication: structure-function correlations, p. 239–268. *In* W. Chiu, R. Burnett, and R. Garcia (ed.), Structural biology of viruses. Oxford University Press, New York, N.Y.
22. **Prasad, B. V. V., R. Rothnagel, C. Q.-Y. Zeng, J. Jakana, J. A. Lawton, W. Chiu, and M. K. Estes.** 1996. Visualization of ordered genomic RNA and localization of transcriptional complexes in rotavirus. Nature **382:**471–473.
23. **Prasad, B. V. V., G. J. Wang, J. P. M. Clerx, and W. Chiu.** 1988. Three dimensional structure of rotavirus. J. Mol. Biol. **199:**269–275.
24. **Prasad, B. V. V., S. Yamaguchi, and P. Roy.** 1992. Three-dimensional structure of single-shelled bluetongue virus. J. Virol. **66:**2135–2142.
25. **Shaw, A. L., R. Rothnagel, C. Q.-Y. Zeng, J. A. Lawton, R. F. Ramig, M. K. Estes, and B. V. V. Prasad.** 1996. Rotavirus structure: interactions between the structural proteins. Arch. Virol. **12:**21–27.
26. **Shaw, A. L., S. K. Samal, K. Subramanian, and B. V. V. Prasad.** 1996. The structure of aquareovirus shows how the different geometries of the two layers of the capsid are reconciled to provide symmetrical interactions and stabilization. Structure **4:**957–967.
27. **van Heel, M.** 1987. Similarity measures between images. Ultramicroscopy **21:**95–99.
28. **Yeager, M., K. A. Dryden, N. H. Olson, H. B. Greenberg, and T. S. Baker.** 1990. Three-dimensional structure of rhesus rotavirus by cryoelectron microscopy and image reconstruction. J. Cell Biol. **110:**2133–2144.
29. **Zeng, C. Q.-Y., M. K. Estes, A. Charpilienne, and J. Cohen.** The N terminus of rotavirus VP2 is necessary for encapsidation of VP1 and VP3. Submitted for publication.
30. **Zeng, C. Q.-Y., M. Labbé, J. Cohen, B. V. V. Prasad, D. Chen, R. F. Ramig, and M. K. Estes.** 1994. Characterization of rotavirus VP2 particles. Virology **201:**55–65.
31. **Zeng, C. Q.-Y., M. J. Wentz, J. Cohen, M. K. Estes, and R. F. Ramig.** 1996. Characterization and replicase activity of double-layered and single-layered rotavirus-like particles expressed from baculovirus recombinants. J. Virol. **70:**2736–2742.
32. **Zhou, Z. H., B. V. V. Prasad, J. Jakana, F. J. Rixon, and W. Chiu.** 1994. Protein subunit structures in the herpes simplex virus A-capsid determined from 400 kV spot-scan electron cryomicroscopy. J. Mol. Biol. **242:**456–469.